CSIRO OCEANS AND ATMOSPHERE
www.csiro.au

# The search for MH370 and ocean surface drift

David Griffin, Peter Oke and Emlyn Jones
report number EP167888
8 December 2016

Prepared for the Australian Transport Safety Bureau

## Citation

Griffin, DA, Oke, PR and Jones, EM (2016). The search for MH370 and ocean surface drift. CSIRO Oceans and Atmosphere, Australia. Report number EP167888. 8 December 2016.

## Copyright

© Commonwealth Scientific and Industrial Research Organisation 2016. To the extent permitted by law, all rights are reserved and no part of this publication covered by copyright may be reproduced or copied in any form or by any means except with the written permission of CSIRO.

## Important disclaimer

CSIRO advises that the information contained in this publication comprises general statements based on scientific research. The reader is advised and needs to be aware that such information may be incomplete or unable to be used in any specific situation. No reliance or actions must therefore be made on that information without seeking prior expert professional, scientific and technical advice. To the extent permitted by law, CSIRO (including its employees and consultants) excludes all liability to any person for any consequences, including but not limited to all losses, damages, costs, expenses and any other compensation, arising directly or indirectly from using this publication (in part or in whole) and any information or material contained in it.

CSIRO is committed to providing web accessible content wherever possible. If you are having difficulties with accessing this document please contact csiroenquiries@csiro.au.

# Foreword

This work is dedicated to the 239 people aboard flight MH370.

# Contents

# Acknowledgments

This work was funded by the Australian Transport Safety Bureau. It drew on models and expertise developed mostly as part of the Bluelink project, a collaboration with the Bureau of Meteorology (BoM) supported by the Royal Australian Navy and OceanCurrent, a component of the Integrated Marine Observing System (IMOS) supported by the National Collaborative Research Infrastructure Strategy (NCRIS). The work would not have been possible without several data sets; we thank 1) the space agencies NASA, CNES, ESA and ISRO and partner agencies NOAA and EuMetSat for satellite altimetry data, 2) the Global Drifter Programme of NOAA, which donated 10 SVP drifters to the project as well as providing access to the entire archive of past trajectories of Indian Ocean drifters, 3) ECMWF, NOAA and BoM for wind and wave data, and 4) Dr Mark Hemer of CSIRO for estimates of the Stokes Drift. We thank Madeleine Cahill (CSIRO), John Wilkin (Rutgers University), Chari Pattiaratchi (University of Western Australia) and Neil Gordon (DST Group) for their constructive comments on drafts of this report.

# Executive summary

This report details the results of a comprehensive attempt to use drift modelling to inform efforts to locate the missing Malaysia Airlines flight MH370 (registered 9M-MRO). It differs from earlier attempts to do this in several important ways, which, along with other developments, have enabled it to come up with a location of the aircraft that is much more precise than we thought was possible.

We have concluded that the northern third (from 36°S to 33°S or perhaps 32°S)[1] of the initial search area uniquely remains prospective. This northern area was partially searched (close to the 7th arc) in the latter half of 2014 and early 2015. Locations outside the searched area, but still within a likely distance from the arc, remain unsearched. The region near 35°S is particularly prospective because there is strong evidence (from Earth-observation satellite data) that this is where, at the time of the accident and for weeks after, the debris field would have been carried north-west for about 500km, away from where the March-April 2014 surface search was conducted and away from the shores of Western Australia (WA). The scenario of a final location near 35°S is the one that is most consistent with:

- the absence of debris findings on the WA coastline
- the absence of debris findings during the aerial and surface search
- the July 2015 arrival time of the flaperon at La Reunion
- the December 2015 and onwards (only) arrival times of debris in the western Indian Ocean.

The uncertainty of this finding has been greatly reduced from what was possible earlier by:

- measuring the wind-driven drift rate of replica aircraft parts alongside oceanographic drifters (whose travel times across the Indian Ocean are well known), and
- using a new ocean model that is informed by very accurate satellite measurements of small perturbations of sea level, yielding estimates of surface currents that have been validated using the global archive of oceanographic drifters.

Are other regions also prospective? If the flaperon had remained the only piece of debris found we would have to say ‘perhaps’, but now many debris items have been found, we can conclude that regions north of 32°S and south of 39°S are both less likely. Drift modelling suggests that debris items originating north of 32°S would probably have been detected by the surface search, and that items would have probably arrived in Africa before December 2015. Regions south of 39°S are not prospective either, because debris from those regions would more likely have turned up on Australian coastlines than west Indian Ocean ones.

[1] Latitudes and longitudes specified as integers, or accompanied by the word ‘near’ in this report have an implied uncertainty of 1/2°

# 1 Introduction

The tragic events of 7-8 March 2014 have been documented many times, so we will not do that again here. Nor will we go over the history of either the surface or sea-floor searches that ensued. We will assume instead that the reader is familiar with the searches and most of the work that has been done in aid of it, and focus this report on our recent contribution to this effort. A glossary is provided in order to reduce the need for lengthy in-line explanations of terminology, while an FAQ section (Appendix A) addresses some questions that would otherwise have broken the flow if addressed in the text.

The search of the sea-floor within approximately 40NM of the 39.3°-36°S segment of the SatCom 7$^{th}$ arc is now nearly complete without 9M-MRO being found. In this report, we attempt to shed light on the question of where the aircraft might be, by drawing on information that is largely independent of the SatCom information that was used to determine the recent search area.

Many parts of 9M-MRO have been found in the western Indian Ocean [link to list], starting with the flaperon that washed up on the shores of Ile de La Reunion on 29 July 2015. We have known for several months that the location and timing of these finds was broadly consistent with the SatCom analysis. However, we were unable to be more precise than that, in part because we could not be sure how the windage (speed of downwind drift) of aircraft parts compared to oceanographic drifters, whose drift-times across the Indian Ocean are known.

Much can be learnt from where and when aircraft parts have been found, once the paths they took can be estimated with some confidence. Much can also be learnt from where and when they have *not* been found. To do this work we have used an ocean surface drift model that we have carefully verified as being fit for this purpose by completing a two-stage calibration exercise.

The first stage involved field deployments of life-size replicas of some of the found parts of 9M-MRO, to measure their windage relative to that of oceanographic drifters.

The second stage involved a careful comparison of the latest revision of our global ocean model with the trajectories of oceanographic drifters. Importantly (as discussed below), this was done using a recent reprocessing of the global drifter trajectory database drogue on/off flag, augmented with data from surface drifters deployed during the surface search by AMSA.

This work has allowed us to estimate the location of the accident site more precisely and confidently than earlier work using either the drifter trajectories alone, or the model alone.

# 2 Methods

## 2.1 Overview

There are strong arguments that flight 9M-MRO entered the ocean somewhere along the 7th arc, within some relatively short distance (~25NM) off-arc (ATSB 2016). In this report, we attempt to refine earlier estimates of the most probable location along the arc (between 45°S and 22°S) of the site using oceanographic techniques.

We assess the chances of locations along the arc being the accident site by calculating paths that aircraft debris would have followed if the impact had been at those locations, then seeing if those paths are consistent with three sets of observations:

1) the extensive aerial and surface search conducted between 18 March and 28 April 2014
2) the absence of aircraft parts found anywhere along the coast of Australia
3) the timing and location of parts of 9M-MRO found on islands in the western Indian Ocean and on the east coast of the African continent.

How does the work presented here differ from existing published attempts (e.g. Jansen et al. 2016, Durgadoo et al. 2016, Trinanes et al. 2016, Pattiaratchi & Wijeratne 2016) to tackle the same question? Existing attempts have expressed their findings for a range of scenarios in which the windage of the aircraft debris is somewhere between 0 and 5%, and Stokes Drift is either neglected or included possibly twice (because of how the models used are calibrated to drifters). This wide range of windage values leads to a wide range of probable impact sites, so one of our highest priorities was to determine the drift characteristics of the parts of 9M-MRO that were recovered in order to estimate their windage factors.

*Rather than trying to measure the windage factors of the aircraft parts in an absolute sense, which is extremely difficult, we measured them relative to oceanographic drifters.*

The next step was to carefully connect our (necessarily) short-term observations of drift characteristics with a model designed for calculating drift trajectories right across the Indian Ocean. For this step, we leveraged the existing archive of the Global Drifter Program, which includes hundreds of cross-Indian Ocean trajectories of satellite-tracked buoys. The final step of the project was to calculate many trajectories across the ocean and analyse them in a way that sifted the robust findings from the inevitable artefacts that models are capable of producing.

## 2.2 Wind effects on the drift of aircraft debris

The effect of wind on the drift of objects floating at the surface of the ocean is much more complex than one might think, so we will certainly not go into all the details here, but instead summarise our approach to taking these important effects into account. We write

$$V = V_c + V_l + V_w \qquad (2.2.1)$$

where $V$ is the velocity of the drifting item, $V_c$ is that of the water, $V_l$ is the 'leeway' velocity and $V_w$ is the velocity due to wave forces.

$V_c$ is the velocity of the surface current. More precisely, this is the velocity of the water very near the surface of the ocean, i.e. averaged over the vertical extent (or 'draft') of the floating object. We will approximate $V_c$ here as

$$V_c = V_5 + V_s \qquad (2.2.2)$$

where $V_5$ is the average over the top 5m of the ocean as estimated by an ocean model and $V_s$ is the Stokes Drift due to waves. In making this approximation we are not explicitly accounting for finer-scale vertical differences of the velocity field or the impacts on the circulation (see Ardhuin et al. 2009, Polton 2005) of the Stokes Drift via the Coriolis-Stokes forcing (which is small compared to the Stokes Drift itself). We will detect and mitigate these omissions by comparing modelled surface velocities with those of real drifters. The Stokes Drift is mostly due to the short-wavelength, locally-generated waves and, importantly, applies equally to all floating objects (of the sizes considered here).

$V_l$ is the velocity of the object relative to the water due to the wind exerting a force directly on the object. It is often written as

$$V_l = w\, U_{10} \qquad (2.2.3)$$

where $w$ is a linear 'windage' or 'leeway' coefficient and $U_{10}$ is the wind speed at 10m height. To allow for non-zero angle between $V_l$ and $U_{10}$, $w$ may be a complex number. If objects drift with a preferred orientation to the wind (as yachts do) then the drift angle will depend on which tack the object happens to be on. Objects with more freeboard (exposure to the wind) and less draft (anchoring them to the water) will have high windage.

$V_w$ is the velocity of the object relative to the water due to the waves exerting a force directly on the object. It depends on the size and shape of the object. If these are such that there is negligible unbalanced force on the object due to interaction with waves, then $V_w$ can be assumed to be zero. If the object absorbs energy from the waves, however, $V_w$ will be non-zero. The waves are driven by the wind, so we will write $V_w$ here as

$$V_w = f(U_{10}) \qquad (2.2.4)$$

The direct ($V_l$) and indirect ($V_s$ and $V_w$) effects are highly correlated, so a common practice (that we adopt in the next section) is to use an effective windage factor to represent the combined effect of Stokes Drift, leeway drift and wave forces. Such empirical windage factors have been tabulated for many items that are frequent subjects of Search and Rescue (SAR) operations. Aircraft parts are not listed in these tables.

Estimating windage factors empirically with any accuracy is very difficult, for several reasons. The velocity of a drifting item is easy to measure, but the velocities of the current and wind, and the height and direction of the waves must also be measured. These quantities are correlated, so many measurements are required along the trajectory of the drifting item, for a wide enough range of conditions, to tease apart the components of the total velocity.

For the present application, we need to know windage factors that are appropriate for calculating trans-Indian Ocean trajectories using model estimates of surface currents, winds and waves, all of which have biases and deficiencies of one sort or another. With this in mind, we have chosen to estimate the windage factors of the aircraft parts using a two-stage process, which takes

advantage of the fact that there already exists a very large number of observed rates of drift across the ocean thanks to the Global Drifter Program (GDP).

GDP drifters are deployed with 6m-long drogues, centred 15m below the surface (see GDP website) so that they do NOT move at the same velocity as an item floating at the surface. The drogues inevitably detach, sometimes long before the drifter stops reporting its position (Lumpkin et al. 2013). At this point, they become more directly relevant to the task at hand. The effective windage factor of these undrogued drifters can be determined quite accurately because the data set is so large. The remaining question is whether their size and shape (30-45cm sphere, 50% submerged with a rubber 'carrot' attached) result in them drifting significantly faster or slower downwind than the found aircraft parts.

## 2.3 Comparing drift rates of aircraft parts and GDP drifters

Replicas of three of the found parts of 9M-MRO were constructed. ATSB built 6 replicas of the flaperon (Fig. 2.3.1) (that washed up on Ile de La Reunion on 29 July 2015), drawing on buoyancy measurements (Fig. 2.3.2) reported by Pengam (2016) and information provided by Boeing. These were life-size and ballasted to replicate as closely as possible the waterline of the real flaperon, while also being close to the same shape. Being made of wood and steel, they are obviously not perfect replicas, and we found that we could not get the trailing edge to float quite as high out of the water as the real flaperon in the extrados-down orientation. Pengam (2016) found the extrados-down orientation to be more stable than the extrados-up orientation, but our replicas do not have this preference to any noticeable degree. We focussed instead on replicating the unequal long-axis waterline of the real flaperon, because this is a likely explanation of why Pengam (2016)'s simulations predicted that the flaperon would drift at 18° or 32° (depending whether the trailing or leading edge was to windward) left of the wind. Needless to say, the replicas were not covered in barnacles, so the extra drag and weight are not replicated. Nevertheless, we think that comparing the rate of drift of these replica flaperons in the real ocean with drifters is probably more instructive than using numerical methods to estimate the windage factor of the real flaperon, which Pengam (2016) found to be 3.3% with the trailing edge to the wind and 2.8% with the leading edge to the wind.

We also constructed replicas of the piece of engine cowling 'Roy' (Fig. 2.3.3) and the fairing. As with the flaperon, care was taken to ensure that the waterline and shape of both were as realistic as possible.

Figure 2.3.1 Replica flaperons at sea off Maria Island, Tasmania, one deployed with the extrados (orange surface) up and one with the intrados (red) up. Both self-oriented with the raised trailing edge to windward. GPS units can be seen in their cut-outs.

Figure 2.3.2 Tank tests (lower) and 3D models (upper) of the flaperon showing equilibrium waterlines in the extrados-down (left) and extrados-up (right) orientations. Figure reproduced with permission of the Direction Generale de L'Armement, from Pengam (2016).

Figure 2.3.3 Replicas of 'Roy' (first seen at Mossel Bay, South Africa on 23 Dec 2015) and the piece of flap track fairing (found on Daghatane Beach, Mozambique, on 27 Dec 2015). GPS units are embedded.

The GDP facility at NOAA AOML kindly donated 10 SVP drifters to the project. We reserved these for deploying in the open ocean once initial experiments in North West Bay near our laboratories in Hobart, Tasmania were complete. When deployed in the open ocean, we cut the drogue free from half of them just below the rubber strain-relief shroud on advice from the GDP that this is where the break usually occurs. We did not attach replica biofouling, so it is possible that our replica undrogued drifters have a slightly higher windage factor than real ones. For the North West Bay work, we used spherical buoys of 45cm diameter weighted with lead to replicate the waterline of the GDP drifters in both drogued and undrogued states. North West Bay is quite shallow, so we used parachute-type sea-anchors (drogues) at 1m depth, in case a greater degree of vertical shear than normally occurs in the open ocean lead to misrepresentative results using drogues at 15m depth.

All items were tracked by fitting them with transponding GPS units. The aircraft part replicas all have two stable z-axis orientations in the water, so we fitted two GPS units to each to ensure there was almost always one unit with a view of the sky. Positions were logged at 5 or 10-minute time intervals. The replica flaperons were also fitted with 3-axis attitude and motion sensors sampling at 25Hz, so their dynamic response to the wind and wave forcing could be analysed numerically as well as being observed and monitored visually. These data are not presented here.

We measured the wind in a variety of ways, ultimately using a Vaisala ultrasonic anemometer mounted atop the cabin of our vessel South Cape, the position and heading of which were continuously logged.

## Results

Preliminary observations, trials and eventually measurements were conducted in North West Bay on 22 and 27 July, 1, 2, 8, 9, 25 and 26 August 2016. These typically comprised two deployments each of about 1 hour duration, during which time the items drifted up to 800m. At first we simply deployed all the items together in a cluster and observed their dispersal. But as it became clear that the relative velocities of the various items were quite predictable, we would deploy the slowest moving items first (two or three drogued drifters) then motor upwind and deploy two or three undrogued drifters (and the replica fairing on one occasion), then finally one or two flaperons at a position about 100m directly upwind of the drogued drifters. The flaperons would almost invariably catch up with and pass close to the other items, then outstrip them. Arranging for the separation between the flaperons and the other buoys to decrease before increasing again did two things: 1) it increased the length of time during which the items were close together, reducing the velocity differences due to spatial variability of the surface current that might be misinterpreted as due to different windage, and 2) it gave immediate confirmation of our hypothesis that the flaperon drifts faster than undrogued buoys, and in the downwind direction rather than in a significant off-wind direction.

The flaperon has a strong tendency to float with the trailing (when fitted to an aircraft) edge or tail raised and presented to the wind. This is true whether the flaperon is floating extrados-up or extrados-down. The tail-up and nose-down orientation is simply a consequence of the weight distribution, but the persistently windward tail surprised us. It is usual for long items to drift with the long axis normal to the wind, but the modelling of Pengam (2016) predicted equal probability of the nose or tail being to windward.

More importantly, the replica flaperons clearly drifted much slower than the rate (3.3% or 2.8% of the wind speed for tail-to-wind or nose-to-wind) predicted by the modelling of Pengam (2016), and at much less than the predicted angle (18° or 32°) to the wind.

While slower than predicted by the modelling of Pengam (2016), the flaperons did drift consistently faster than all the other items. This was most strikingly apparent [link to video] when there was just a gentle breeze. We attribute this to the $V_w$ term in equation 2.2.1, because there were always small, short wavelength waves in North West Bay even when the breeze was very gentle. The flaperon was clearly interacting with the waves, locally modifying them and presumably absorbing momentum as each little crest slapped against the raised tail. The relative velocity of the flaperons and undrogued drifters varied from day to day but was usually in the vicinity of 10cm/s for low wind speeds and in the direction of the wind. This translates to a potential additional drift in excess of 8km per day.

Under high wind conditions the flaperons drifted closer (within 5cm/s) to the speed of the undrogued drifters and in the same (+/-10°) direction. As the wind rose to 20kt, the raised tail of the flaperon would come closer to vertical [link to video] with each wave until a gust would pitch it over, leaving the flaperon with the nose instead of the tail to the wind. Within a minute or two, it would yaw until the tail was windward again and continue on until the next time a wind gust combined with a wave to pitch it over again. We assume that these interactions with the waves are too complex to be represented by the numerical simulation of Pengam (2016) and that this explains the discrepancy of the observed and modelled rate and direction of drift.

The fairing was also deployed on a few occasions in North West Bay, where we very quickly learnt that its two stable orientations had completely different rates of drift. Initially deployed with its inner (concave) surface facing up, the fairing drifted off so rapidly we decided to retrieve it immediately before losing it. We never saw the wind pitch it over but formed the opinion that this was very likely, because its edges were vertical in the air and caught the wind as the fairing crested a wave. Deployed with the concave surface facing down, those edges caught the water rather than the wind and its rate of drift was much less, and indeed indistinguishable from that of the undrogued drifters.

The next phase of fieldwork comprised indefinite deployments into the open ocean off the east coast of Tasmania. These were conducted on days when winds were forecast to carry the items eastward away from land.

The first open ocean deployment was on 4 October 2016. Unfortunately, the GPS units on the flaperons failed to work on this occasion because of a problem with the additional batteries fitted. There was no such problem with the Roy and fairing replicas. These followed the drift of the undrogued GDP drifters quite closely (see Fig. 2.3.4), drifting 40km downwind over a 48h period, compared to the 45km covered by the undrogued drifters. Meanwhile, the northwards current carried all the items about 80km northwards. Note how close together the two undrogued GDP drifters and two drogued drifters remained, giving us some confidence that the separation of the 4 different types of item was not due to turbulence in the ocean, but largely due to their different windage factors.

The second open ocean deployment was on 18 October 2016 (see Fig. 2.3.5) and on this occasion everything transponded, if intermittently in some cases. (We attribute this intermittency to the fact that replica fidelity was our highest design priority, not platform stability for the sake of

reliable satellite communication.) The flaperon, Roy and fairing replicas all remained very close to the two undrogued GDP buoys for the first 24h but then diverged slightly, only to rejoin them later on. This suggests that the two undrogued drifters may have been travelling along a convergent front – it is impossible to be sure.

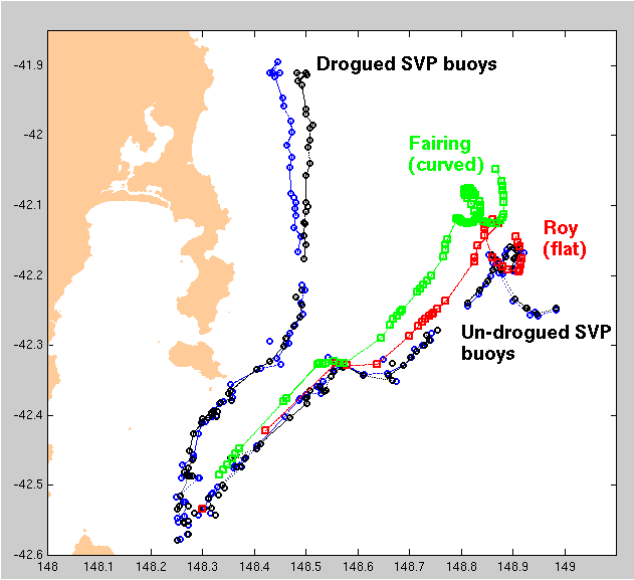


Figure 2.3.4 Trajectories over 48h of 6 items deployed near Maria Island, Tasmania on 4 October 2016. Winds were ~20kt from the NW and SW as evidenced by the separation of the 4 undrogued items from the 2 drogued GDP drifters. The effective windage of the fairing and Roy is evidently just slightly less than that of the undrogued drifters.

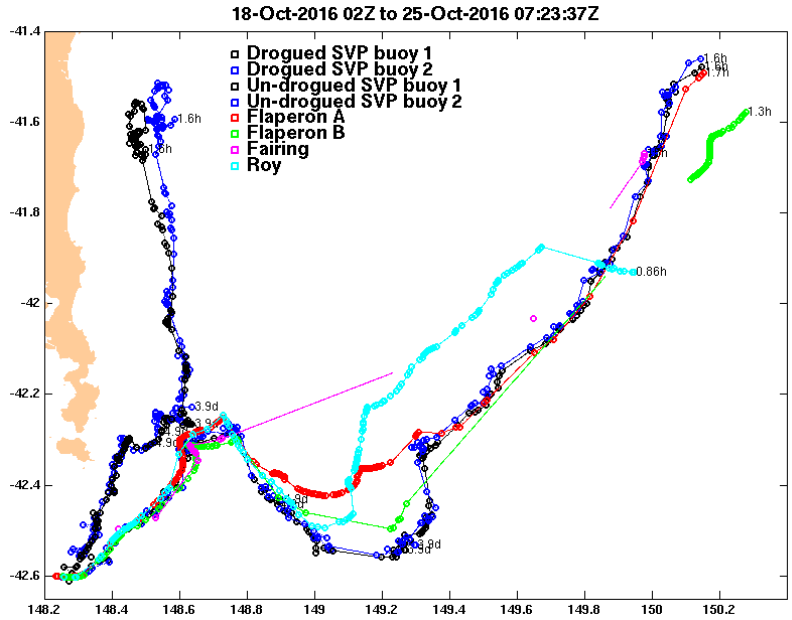


Figure 2.3.5 Trajectories over 7 days of 8 items deployed near Maria Island, Tasmania on 18 October 2016. Winds were mostly quite strong (>15kt) and from the NW - SW except during the passage of fronts. The effective windage of the flaperons (and other aircraft parts) in these conditions is evidently very similar to that of the undrogued drifters.

The winds during both these offshore deployments were fairly strong (15-25kt) for much of the time, so there was essentially no opportunity to verify in the open ocean the higher drift speed of the flaperons observed under the low-wind conditions in North West Bay. In the following work, therefore, we will reconcile these observations by assuming that the flaperon drifts at 10cm/s in the direction of the wind for all wind speeds less than 10m/s, then at the same speed as undrogued drifters (which we will assume below to be a constant fraction near 1% of the wind speed) for higher wind speeds. An equivalent way of expressing this is to say that the extra downwind speed of the flaperon reduces linearly from 10cm/s in 0m/s of wind, to 0cm/s in 10m/s of wind.

Analyses of these data sets are continuing, and more deployments are planned. But at this point it is fairly clear that the replica aircraft parts all have effective windage factors that are close to that of the undrogued drifters, despite the differences in the size and shape of the various items. Recalling that the effective windage factor is the sum of the Stokes Drift, leeway and wave force contributions, this suggests that both the leeway term (and therefore the true windage factor) and wave force terms are small compared to the Stokes Drift (unless the wind is very weak).

## 2.4 The windage factor of undrogued drifters

Having established that the effective windage factor of small pieces of aircraft debris is close to the effective windage factor of an undrogued drifter, we now want to estimate this parameter as accurately as possible so that when we simulate the drift of a piece of aircraft debris using particular ocean and atmosphere models it will take the same time to cross the Indian Ocean as an undrogued drifter would have in 2014-15. This means we should estimate $w$ using those same particular ocean and atmosphere models, using data for 2014-15. The reason for this is that this estimation problem is sensitive to potential systematic biases (offsets as well as scale factors) in the particular ocean and atmosphere models used for estimating $V_5$ and $U_{10}$ when solving

$$w = \frac{V - (V_5 + V_s + V_w)}{U_{10}} \tag{2.4.1}$$

in a least-squares sense.

The ocean model we use here is known as BRAN2015, being the 2015 version of the Bluelink ReANalysis. Bluelink is a partnership between CSIRO, the Bureau of Meteorology and the Royal Australian Navy. ‘Reanalysis’ is a term borrowed from meteorology to distinguish a hindcasting model that closely fits available observations, from a forecasting model that makes a genuine prediction into the future by stepping forwards from an analysis of available observations. An analysis (or done later, with more data, a ‘reanalysis’) can be thought of as the result of using the full physics of an ocean or atmosphere model to interpolate between the fairly sparse available observations of some of the state variables of the model. The state variables of BRAN2015 are the velocity, temperature and salinity for 54 layers in the vertical (which are 5m thick at the surface), at almost 5.5 million points on the globe at 0.1°x0.1° (latitude x longitude) intervals, plus the sea surface elevation on the same grid. The data assimilated comprises satellite estimates of the sea surface elevation (by altimetry) and temperature (by radiometry), and subsurface estimates (predominately by Argo robotic profiling floats) of temperature and salinity. The model is also forced at the surface with 3-hourly estimates of the fluxes of heat, momentum and precipitation-

evaporation provided by the ERA-Interim (Dee and Uppala 2009) atmospheric reanalysis, which is the atmospheric model used here. For details of an earlier version of BRAN2015 see Oke et al. (2013a,b). For estimates of the near-surface Stokes Drift, we use an extension of the CAWCR Wave Hindcast.

The quantity $V$-$V_5$ is the velocity of a drifter relative to the hydrodynamic model's estimate (which does not include the Stokes Drift) of the surface current. The spatial variability of this quantity, averaged over all undrogued drifter velocities for 2014 and 2015, has a very clear pattern that very closely resembles the wind velocity evaluated and averaged in the same way, as shown in Fig. 2.4.1. It also very closely resembles (as seen by Rascle and Ardhuin 2013) the Stokes Drift evaluated and averaged in the same way, as also shown.

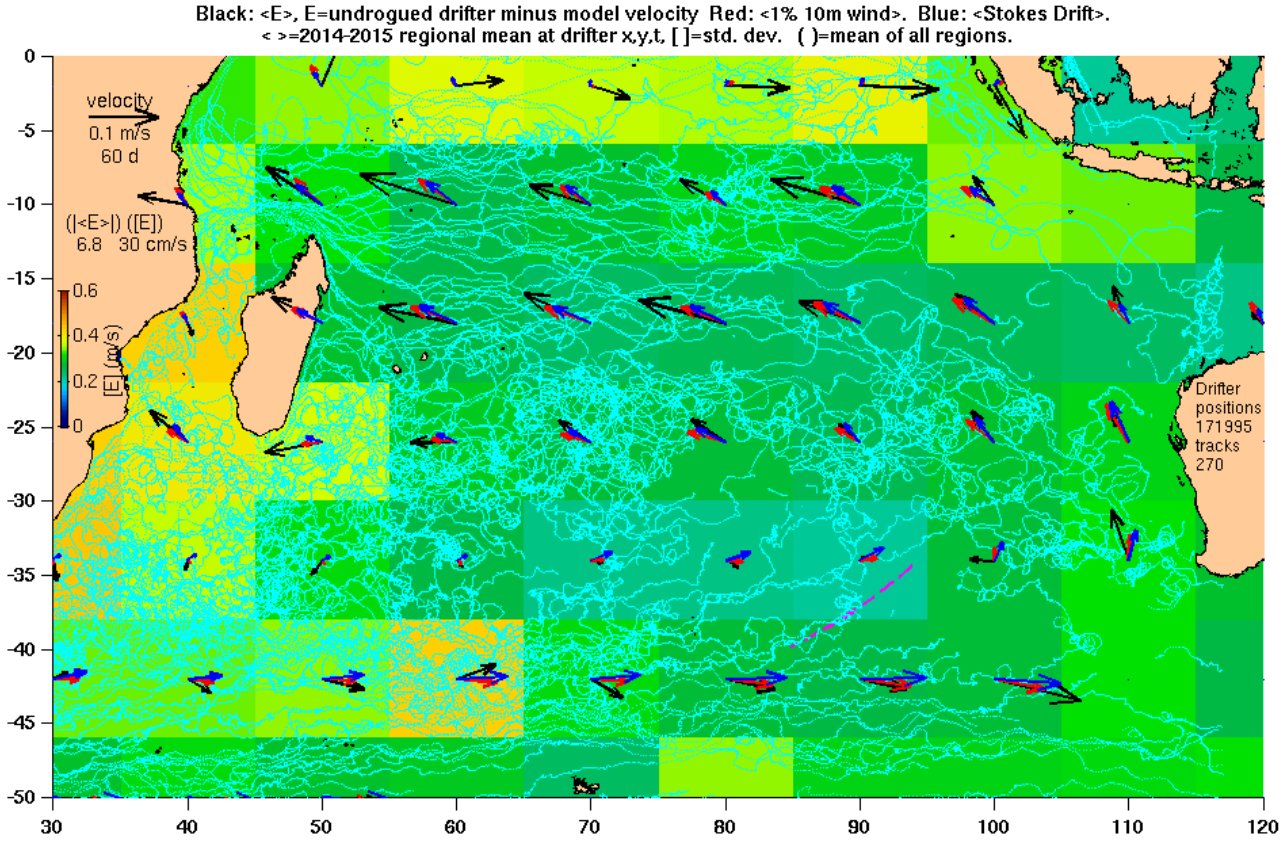


Figure 2.4.1 Black arrows and colour-fill show the mean and standard deviation of the difference, respectively, of undrogued drifter and model (at drifter time and location) velocity, averaged within 8°x10° regions for 2014 and 2015. Cyan lines are the drifter trajectories. Blue arrows show the mean Stokes Drift calculated by the CSIRO-BoM implementation of WaveWatch III for 2014 and 2015, evaluated and averaged as above. Red arrows show the similarly-processed ERA-Interim 10m wind scaled by 1% for comparison. Aside: similar plots for [drogued] and [SLDMB] drifters.

Solving equation 2.4.1 (with $V_w$ set to zero, as appropriate for drifters) for $w$ leads to very uncertain estimates, even with such a large data set as we have used. The reason is that $V - (V_5 + V_s)$ is uncorrelated with $U_{10}$ because $V_s$ has accounted for most of the wind-correlated part of $V$. We find, however, that the wind has a slightly higher correlation with $V$-$V_5$ than the Stokes Drift does, so we chose to use this as a proxy for the Stokes Drift for predictive modelling purposes. Defining an effective windage factor

$$w_e = \frac{V - V_5}{U_{10}} \qquad (2.4.2)$$

as the one that we estimate without explicitly accounting for Stokes Drift, we find that the value that minimises the unexplained velocities of the drifters is 1.2%. But the fact that the Stokes Drift alone can almost completely account for $V$-$V_5$ (averaged over large intervals of time and space) is significant. It implies that the 'true' windage $w$ of an undrogued drifter is small (i.e. much less than 1.2%), which says that the downwind motion of the drifter is mostly due to the wind-driven waves (via Stokes Drift) rather than the wind acting directly on the exposed portion of the drifter (as seen by Rohrs et al. 2012). This implies that any deeply submerged, similarly sized object floating right near the surface of the ocean will drift downwind relative to the Eulerian mean of the surface layer of the ocean (which is what an ocean model without waves simulates) at much the same speed as an undrogued drifter.

## 2.5 A de-biased estimate of ocean surface velocities

The GLD drifters are undrogued for about half of their lives. The earlier half when their drogues are still attached is also of value to us for the present task, because their estimates of $V$ (at 15m average depth) can be used to estimate the spatial pattern of the remaining unexplained velocity of drifters. For this task we combined the velocity data from three types of drifters: GDP drogued and undrogued, and also the many SLDMB drifters deployed by AMSA during the surface search in an area with otherwise few observations. We subtracted BRAN2015 velocity at appropriate depth level, and windage for undrogued drifters. Fig. 2.5.1 shows that drifters go east along the equator and west in a band between 10° and 15°S faster than BRAN2015 estimates. We think we have now found the cause of this systematic error in BRAN2015, but it will take a year or more before a new version of BRAN will have this fixed. In the meantime, we have used a de-biased version of the BRAN2015 surface velocity archive for simulating trajectories, by adding the velocity field shown in Fig. 2.5.1 to the daily-averaged BRAN2015 surface velocity estimates.

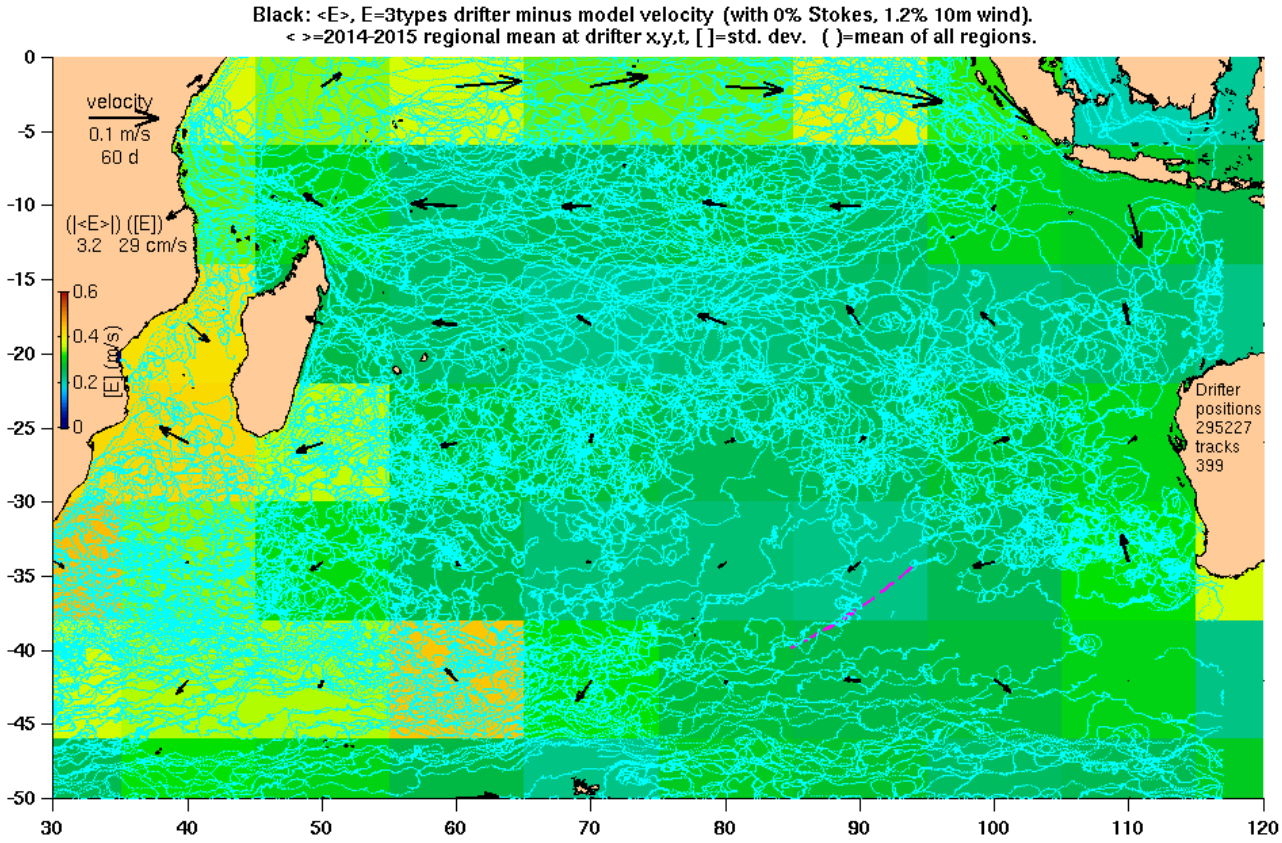


Figure 2.5.1 Binned estimates of the time-mean (vectors) and standard deviation (colour-fill) of the remaining unexplained velocity of 3 types of drifters (drogued and undrogued GPD drifters, plus AMSA's SLDMBs deployed during the surface search). We interpret this error velocity field E as a model bias and remove it before proceeding, noting that the largest values are distanced from locations of present interest. The all-area spatial mean of the magnitude and standard deviation of E are 3.2cm/s and 29cm/s. The similarly-binned velocity of the drifters has an average magnitude of 13 cm/s, and standard deviation of 35cm/s, as shown in the [online Appendix].

## 2.6 Calculating paths from velocities

Equipped with an archive of daily estimates of surface current velocity and wind, it is relatively straightforward to calculate a trajectory either forward or backwards through time by stepping the position of an item along at the vector sum velocity due to current, wind and, in the case of the flaperon, wave forces. This can be done for huge or modest numbers of items, and with or without an additional randomly-oriented step to mimic small-scale dispersive velocities that are unresolved by the velocity field being used. We believe that adding such random velocities adds little value to a modelling exercise such as this one because they do not substitute for properly resolving the small-scale features. We have therefore not added them. A more important issue is the one of how to calculate trajectories from velocities. Ocean flows typically have high curvature that is barely resolved by a 0.1° grid, so it is important to ensure that trajectories follow this curvature rather than the local tangent. We therefore step along at just a few hours at a time, using a 4$^{th}$-order Runge-Kutta integration scheme.

# 3 Paths of debris from potential accident sites

## 3.1 Qualitative analysis

Let us look first at the 'big picture', to get a sense of how fast the winds and currents of the Indian Ocean transport material in a generally anti-clockwise direction. We will look at simulated trajectories of items that were distributed along the SatCom 7$^{th}$ arc from 45°S to 22°S on 8 March 2014. Fig. 3.1.1 shows the positions at 3-month intervals of these items, coloured by starting position. They all drift with the same effective windage factor as undrogued drifters, so they are representative of medium-sized (less than 1m), deeply-submerged debris items such as the various pieces of cowlings and fairings found on the African coastline from December 2015 and into 2016. Fig. 3.1.1 includes an outline of the sea-floor area that has been searched, as of October 2016, for reference. We will refer to this as the 'searched area'.

The red-coded (northern-most start points) and blue-coded (southern-most start points) items moved the furthest in the first 3 months, the former generally north-west because of the trade winds and the South Equatorial Current and the latter generally east because of the westerly winds and eastward flow along the Sub Tropical Front. Magenta and black items (starting from points spanning the northern and southern halves respectively of the searched area) moved much shorter distances because of the weaker and/or less persistent winds and currents in this intermediate band of latitudes.

By September 2014 the red items have reached the northern tip of Madagascar and are about to reach Tanzania. Many blue and green-coded items are leaving the computational domain, presumably towards Tasmania. A few magenta and yellow-coded items have come close to Perth, Western Australia due to the westerly winter winds in that region.

By December 2014 there are many red-coded items from Kenya to Mozambique and many green and cyan-coded items along the coast of Western Australia from Perth to Shark Bay. But no aircraft debris was found as early as December 2014 anywhere in the western Indian Ocean, or ever on the coast of Australia, so this modelling suggests that the northern-most (red-coded) and southern-most (green, cyan) regions are less likely to have been where the aircraft impacted. In the next section, therefore, we will look more closely at a narrower range of possible accident latitudes. The magenta and black-coded items are still in the general vicinity of the 7$^{th}$ arc, but further north than their initial position near the searched region.

The main changes from December 2014 to March 2015 are that a few of the items near Africa have travelled quickly south in the fast, narrow Agulhas current, while the items that were near Western Australia have been blown back out to sea by the summer winds.

March to June 2015 is essentially a repeat of what we saw in March to June 2014, but this time it is items of various origin instead of just the red-coded ones making the westward trip in the South Equatorial Current.

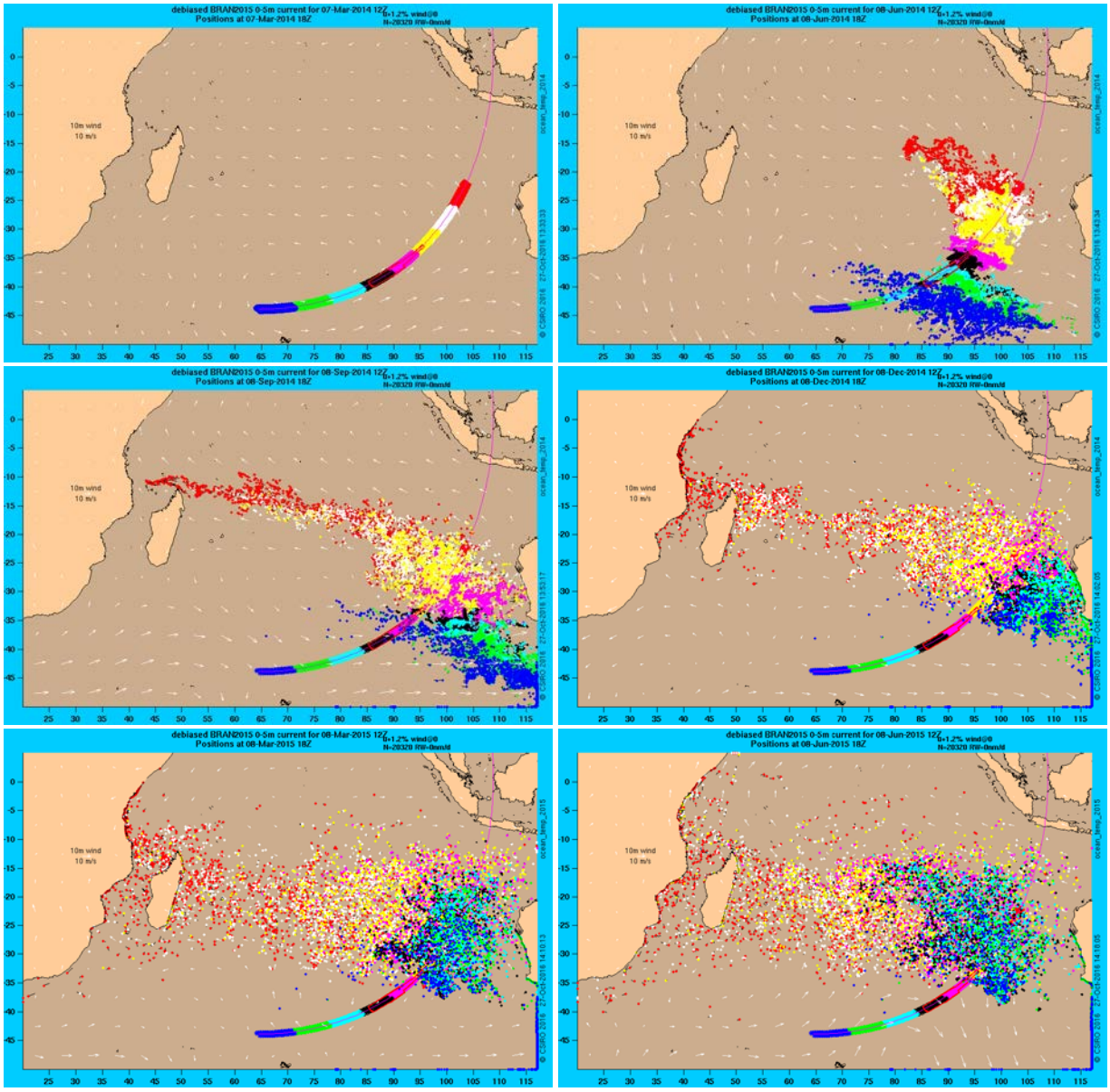


Figure 3.1.1 Computed positions at three-month intervals of many hypothetical items that were within 45NM of the SatCom 7th arc on 8 March 2014 as shown in the first (and subsequent) panel. The items are assumed to move subject to the combined influence of wind, waves and current, to replicate as closely as possible the drift of the small ('non-flaperon') pieces of the aircraft found in Africa. See also the online Appendix for [stills and animations of daily positions], or the same with the [speed of ocean currents] shown as the background colour.

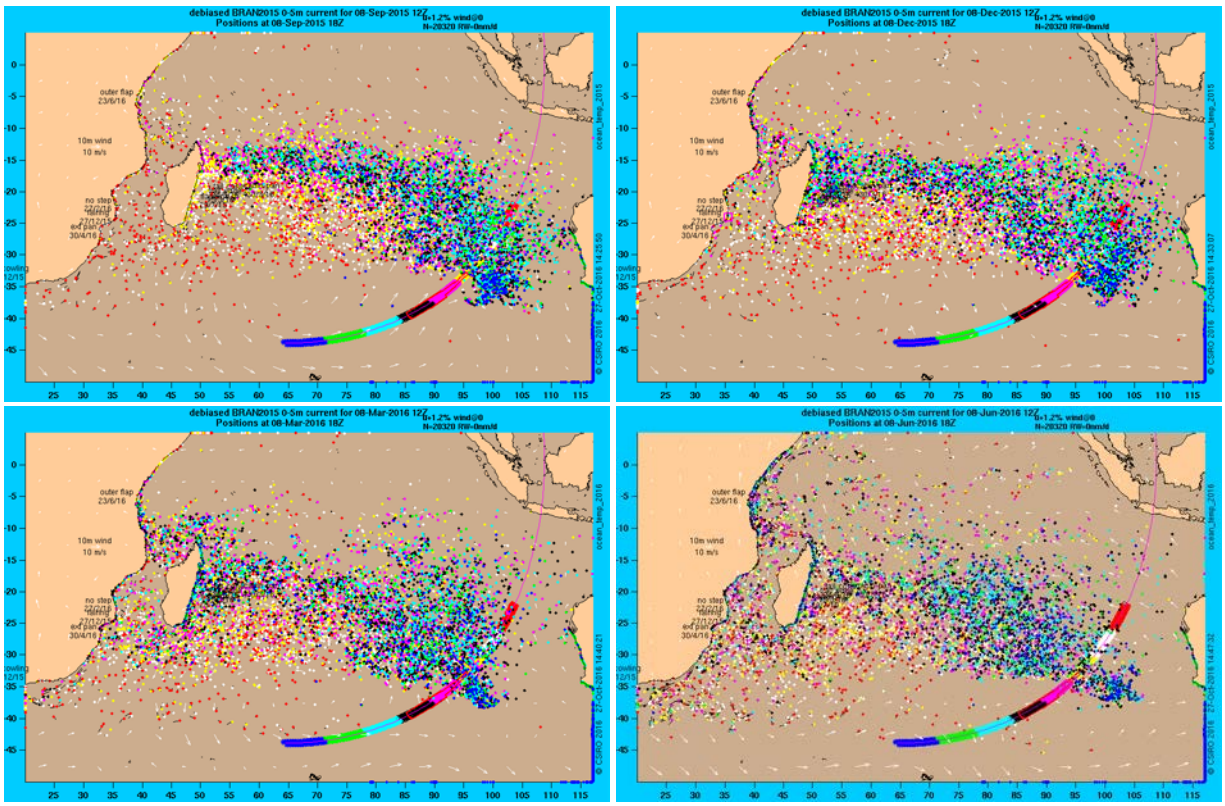


Figure 3.1.1 (continued)

By September 2015 those items travelling west have reached Madagascar, most passing north of Ile de La Reunion. There are many large eddies in the current, possibly diverting items southward, so the arrival of the flaperon at Ile de La Reunion in July 2015 is not inconsistent with this simulation, as was noted at the time using a preliminary but similar model. The fairly wide range of possible origins of the flaperon was also noted at the time. The purpose of this report is to see if a closer examination of this question can narrow down the range.

By December 2015 the number of items along the coast of Africa is greater than in September, which is consistent with the fact that December 2015 was when the engine cowling 'Roy' was photographed in Mossel Bay, South Africa and the fairing was found in Daghatane Bay, Mozambique. The wide distribution of items along the coast of Africa is due to the fast boundary currents that flow along this (and many other, but certainly not all) continental margins.

The final two panels of Fig. 3.1.1 show continued circulation of items, and an increasing number of items off Tanzania. This is consistent with the outer flap being found there in June 2016, without ruling out a significantly earlier date of arrival.

To conclude this initial discussion of these modelled trajectories, we note that about half of the items are predicted to still be, in June 2016, in the eastern half of the southern Indian Ocean – some not far from their points of origin in 2014. This is because of the turbulent nature of the ocean circulation. Chance encounters with eddies carry some items backwards against the mean flow. The consequence is that potentially many parts of the aircraft (that are still floating) are yet to wash up on any coastline, and may not do so for years.

### Why was the flaperon the first item to be found?

Recall that the items depicted in Fig. 3.1.1 represent items of miscellaneous debris, i.e. drifting at the speed of undrogued drifters. In Section 2 we concluded that the flaperon drifted faster than undrogued drifters under low wind conditions. Fig. 3.1.2 shows that the consequence of this extra drift speed is that in July 2015 the modelled positions differ by 10 or 15° of longitude. The flaperon-like items are only about 1 month ahead of the non-flaperon-like items, as can be seen by comparing the 1 August positions of non-flaperon items with 1 July positions of flaperon-like items (see links to the online Appendix in the caption of Fig. 3.1.2). We also mentioned in Section 2 that the real flaperon may have drifted slightly faster than our replicas if it floated higher in the water. This would increase its lead, but probably not by a factor of 5, so we conclude that the extra speed of the flaperon does not clearly account for the 5-month gap between the flaperon's discovery and subsequent finds. The position of landfall 30° east of the coast of Africa is probably the dominant factor explaining the earlier date.

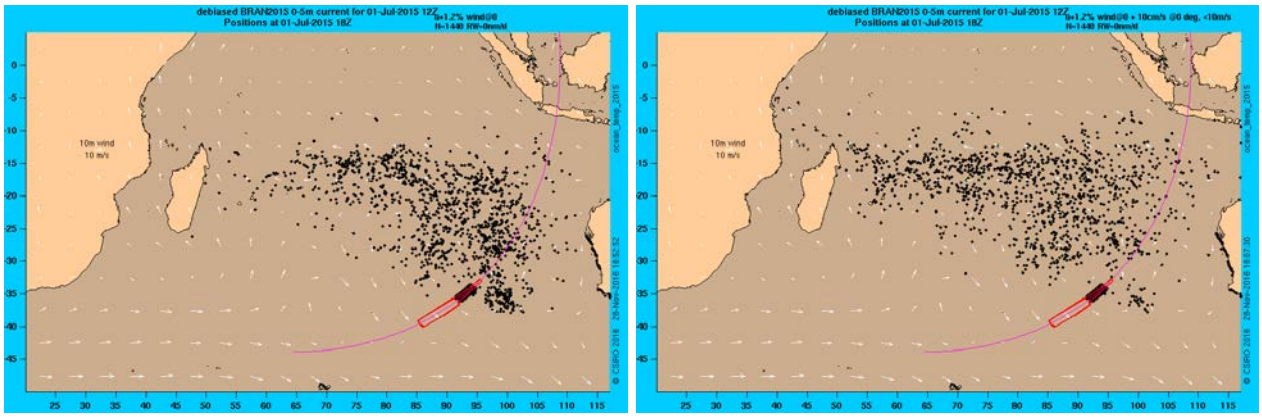

Figure 3.1.2. Comparison of modelled positions, on 1 July 2015, of non-flaperon (left) and flaperon-like (right) items that were between 36°S and 34°S on 8 March 2014 (i.e. a subset of the initial positions used for Fig. 3.1.1). The flaperon-like items drift slightly faster than other items, but only when winds are less than 10m/s, as discussed in Section 2. See also the online Appendix for stills and animations of daily positions of [non-flaperon] and [flaperon] items or the same with the [sea surface temperature] shown as the background colour (for the non-flaperon items).

## 3.2 Quantitative analysis

It is not easy to assess the density of the variously-coloured items in Figures 3.1.1 and 3.1.2, or to track this as a function of time by watching the animations, because the 8 variously-coloured items from the many closely-spaced hypothetical accident sites are all intermingled. For a more quantitative analysis that can be summarised on one page we proceed as follows. First, we divide the 42-26°S segment of the 7$^{th}$ arc into 48 bands of equal meridional extent. This allows us to estimate the likelihood of potential accident sites with relatively high spatial resolution (1/3° of latitude). Next, we select the bounds of the significant destination areas: the shores of Africa (where we know many items arrived, starting December 2015), Ile de La Reunion (one item in July 2015) and the coast of Western Australia (no items). Their areas are quite large because we accept that the model is not perfect, so trajectories that go near somewhere like Ile de La Reunion are equivalent to those that actually hit it. Similarly, the physical processes that determine whether items strand on coasts or travel long distances along them cannot be modelled accurately, so we

take either outcome as equivalent. Then we step through the history of the model a month at a time, and calculate the probability of being in each of the destination areas, given that a trajectory started in one of the hypothetical water entry regions. This can be thought of as the probability of *going* somewhere, and is simply the number of trajectories to the destination divided by the number of trajectories starting in the latitude band. (It is *not* the number of linking trajectories divided by the total number of trajectories from all sources passing through the destination – that is the probability of *being from* somewhere). These probability maps are shown in Fig. 3.2.1 for both the flaperon and non-flaperon trajectories.

The earliest-possible arrival month of the flaperon at La Reunion, according to this model, ranges from September 2014 if the aircraft entered the ocean at 30°S to September 2015 if the entry was at 42°S. The most-likely arrival month is less varied: August 2015 for northern sites and November 2015 for southern sites. Viewed another way: the July 2015 arrival time is generally increasingly consistent with this model for increasingly northward sites. July 2015 is earlier than expected for all latitudes except the 30°S outlier, and the degree to which one considers this to rule out those latitudes depends on how typical we would like to assume this single flaperon trajectory to have been.

It is impossible to know if the real flaperon made a particularly fast or slow trip across the ocean, or followed a likely or unlikely path through the turbulence, so we can only cautiously conclude, considering only the *single* flaperon arrival date, that 1) the model is not really consistent with the site being south of 36°S (which agrees of course with the aircraft not being found there), 2) sites from 36-33°S are moderately consistent with the model, and 3) sites north of 33°S are quite consistent.

The subsequent findings of several more items on the coast of Africa is another matter. The arrival time of the first two items found, given that many more followed, implies quite strongly that for most potential sites north of 33°S it is very odd that no debris was found in the six-month or longer period before December 2015. This argues quite strongly that the water entry was south of 32°S or 33°S.

The absence of debris on the Australian coastline is also useful information. The observer density is low compared to most shores in the west Indian Ocean but awareness of the significance of a find, and likelihood of reporting that find, is presumably high. This absence of findings argues against three latitude bands as potential entry locations. These are near 33-35°S, 36-37°S and 39-42°S, leaving sites north of 32°S and bands around 35-36°S and 37-39°S as being more consistent with the absence of Western Australia (WA) debris findings.

The probabilities of going to WA and Africa are not independent, but anti-correlated for the mid-range of potential accident site latitudes, suggesting that for these regions of the arc, the alternative destinations of debris are few: east or west. The 35°S band of reduced probability of going to WA shows up in the flaperon's La Reunion destination panel as a local maximum of the probability, but four months later than the flaperon actually arrived there. There is remaining uncertainty over how fast the real flaperon drifts, in addition to the uncertainty of how typical this particular trip was. The former source of uncertainty is relatively easy to deal with, by generating trajectories with the flaperon's windage factor increased beyond the values that were consistent with our field tests of replicas. Fig. 3.2.2 shows that doubling (from 10m/s to 20m/s) the upper limit of the wind speed below which the flaperon drifts faster than an undrogued drifter brings the

most likely arrival time at La Reunion forward by 4 months but leaves the 35°S local maximum of probability in place.

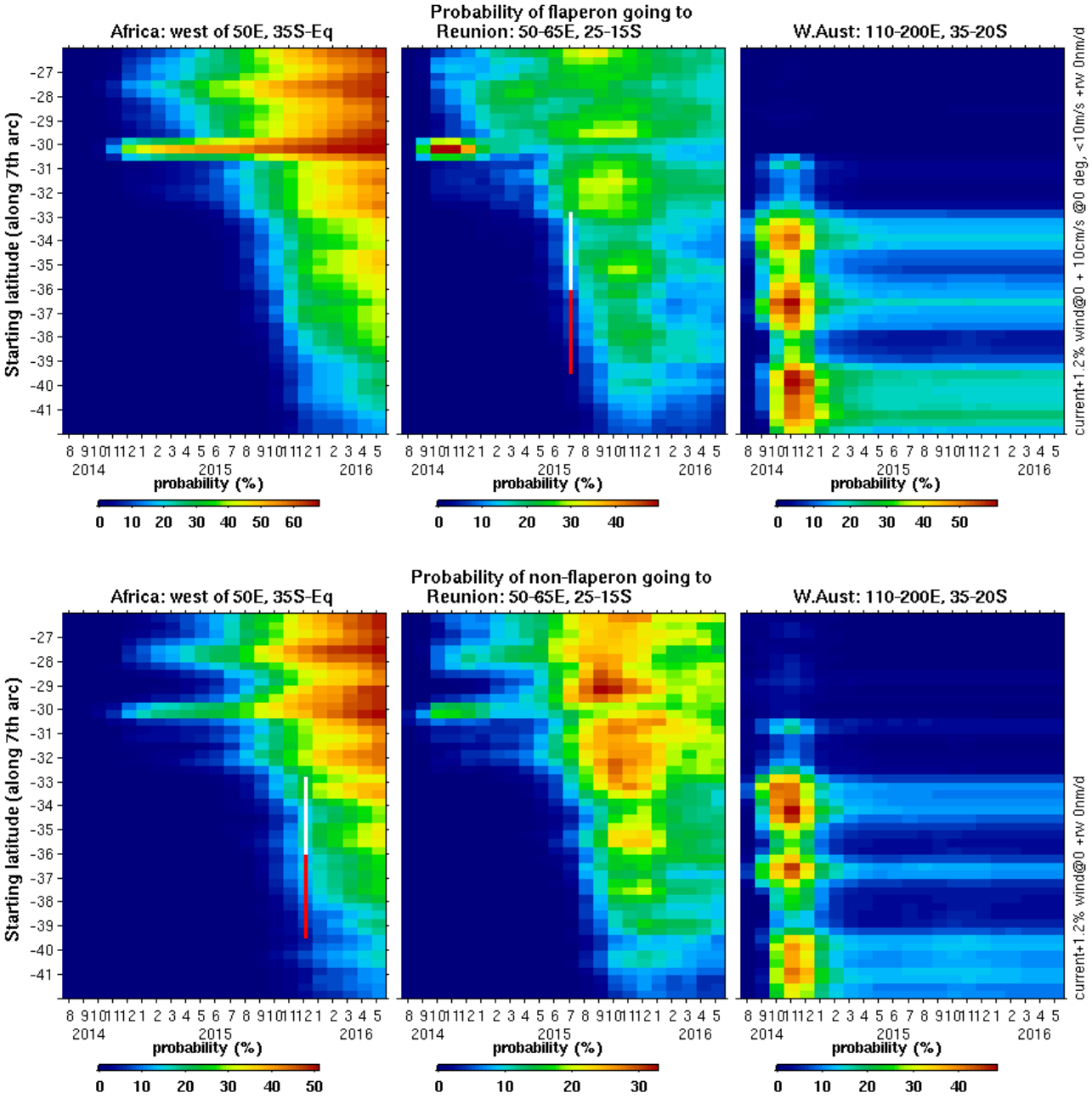


Figure 3.2.1 Time-dependent trajectory probabilities for flaperon (upper row) and non-flaperon (lower row) debris items. The modelled trajectories link starting points along the SatCom 7th arc (binned by latitude shown on the y-axis) with three destination regions described along the top of the panels. Time is along the x-axis. The colour indicates the number of linking trajectories (for each month) divided by the number of trajectories that started in each latitude band. If items stop moving because they are beached, they count towards the probability for all time after they beach. Two lines are superimposed on the maps, in July 2015 for the flaperon map and December 2015 for the non-flaperon map. The red section of the line spans the latitudes of the 7th arc that have been widely searched (out to ~ 40NM either side). White spans the latitudes that have only been searched within 10 to 21NM of the arc.

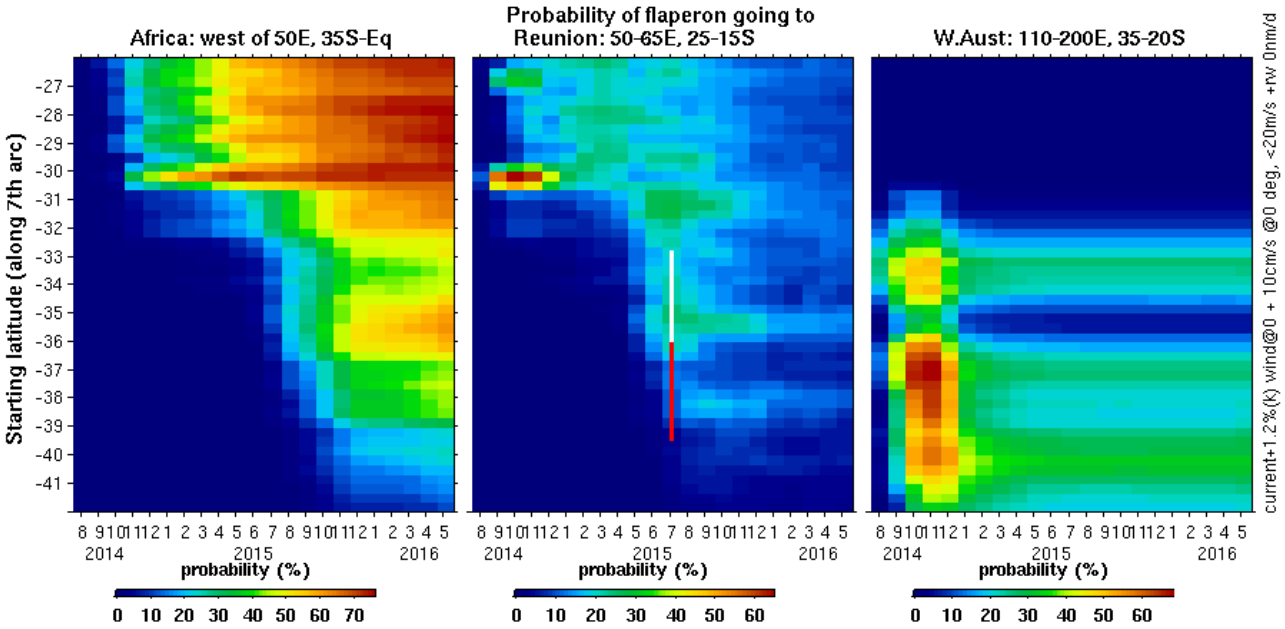


Fig 3.2.2 Flaperon trajectory probability map using a windage factor that is higher than observed, to demonstrate sensitivity of results to possible under-estimation of this parameter.

## 3.3 Importance of the initial direction of movement of debris

How could the probability of going to WA be so dependent on the starting latitude? The key to understanding this lies in understanding how the surface of the ocean was moving at the time of the accident.

It appears, from our modelling, that the initial direction of movement had a lasting impact on the long-term trajectories, much like one's choice of train does at the station. This is a result that we did not, at first, believe could be real, because the ocean is so full of eddies. The analogy is more appropriate if the trains are all going in much the same direction, but some are express services, taking shorter routes.

The ocean's eddies, fronts and currents are represented fairly realistically in our model, thanks to all the satellite data that it relies on. The satellite altimeter data tells us, via the model, that there were alternating bands of eastward and westward flow, including two prominent ~150km-wide bands of westward flowing surface current crossing the 7$^{th}$ arc in March 2014 – one near 35°S and one near 30°S (Fig. 3.3.1). The current near 35°S carried floating items about 500km west before turning north (Fig. 3.3.2). The location of the starting points of the modelled trajectories that are influenced by this westward current is apparent in Fig. 3.3.3 which shows that trajectories starting near 35°S or north of 32°S have reduced chance of going near WA and greater probability of passing by La Reunion at dates acceptably close to the arrival time of the real flaperon. We allow here a time window of +/- 50d to account for two things: 1) the real flaperon's trip may not have been representative of other identical items also in the water 2) our replica flaperons may drift slower than the real one.

It appears that this initial 500km westward displacement was enough to set that water on a route to the western Indian Ocean that was shorter than the routes taken by neighbouring bodies of

water (shown in the **[on-line Appendix]**) that moved initially east. Bands of water flowing eastward towards WA on 8 March 2014 were more likely to enter the eddy field of the Leeuwin Current, where the combined influence of winds and currents decided whether any floating debris was carried ashore, or continued slowly north until joining the South Equatorial Current. Similarly, the current at 30°S (whose existence is independently confirmed by the trajectory of a GDP drifter) set many modelled trajectories on straight, fast paths across the Indian Ocean, leading to the band of anomalously-short (compared to adjacent latitudes) modelled travel times.

The fact that no aircraft debris was ever found on Australian shores suggests that the aircraft is more likely to have entered the water in *one of* the latitude bands where the flow was westward. The absence of African findings before December 2015, however, argues against the 30°S band.

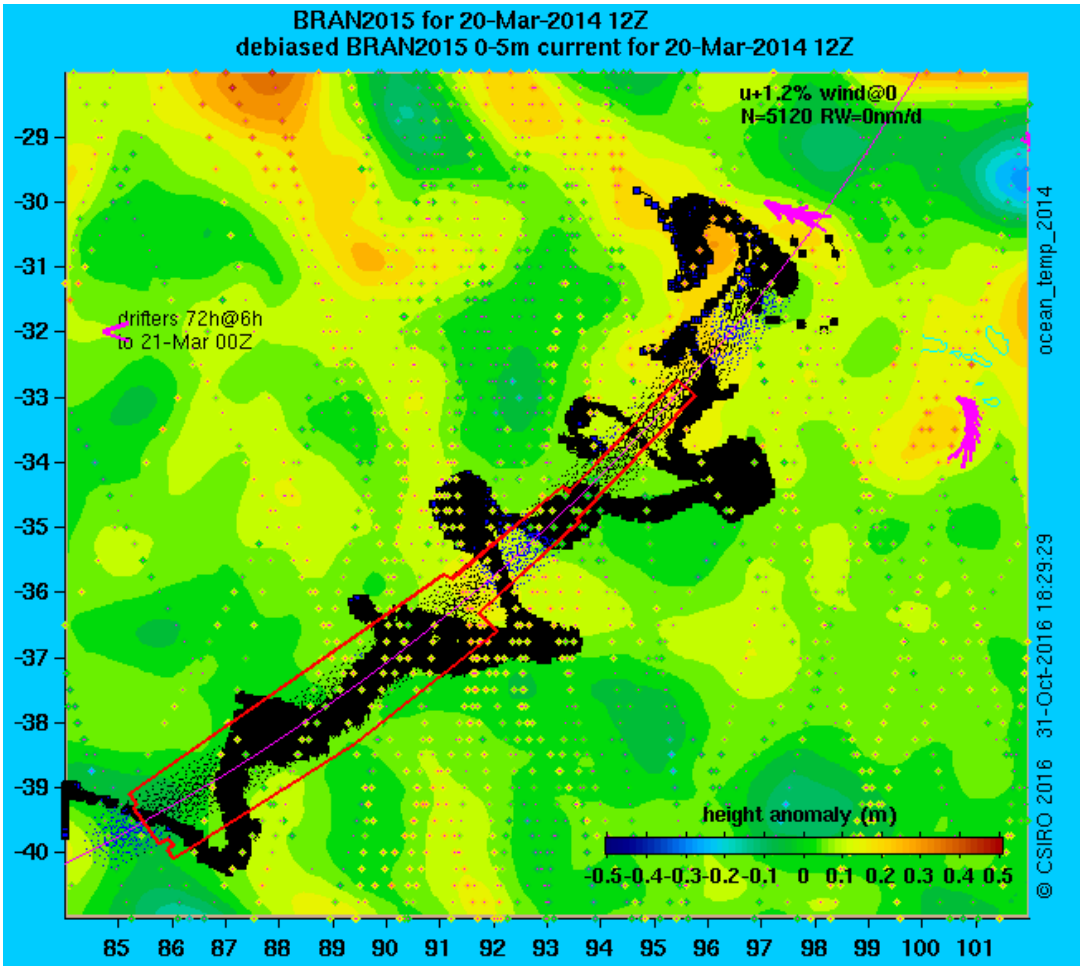


Figure 3.3.1 Modelled positions on 20 March 2014 of potential debris items, overlain on the oceanographic synoptic map for the day. The starting locations are coloured blue if the initial movement was NW and black otherwise. Surface currents tend to flow along contours of equal sea-surface elevation above a geopotential surface ('height anomaly'), just as winds blow along isobars. The satellite altimeter measurements of height anomaly that were provided to the model are shown as coloured diamonds with dark central dots. The trajectories of two GDP drifters that happened to be in the region are shown as magenta arrow heads. They travelled with positive sea level on their left, as expected, providing independent confirmation of the model. The searched area is outlined in red. For other dates, see the [Online Appendix].

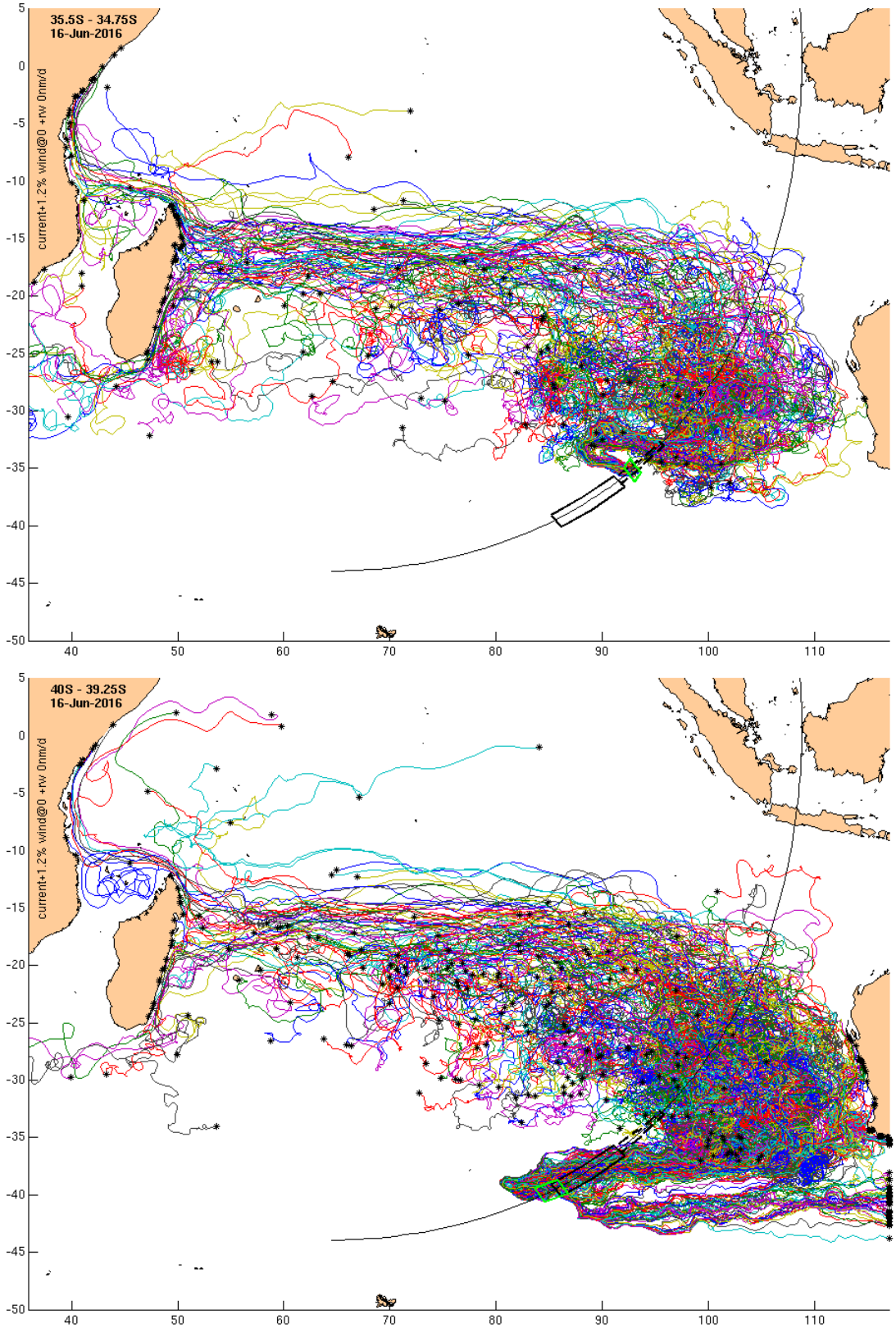


Figure 3.3.2 Trajectories from 8 March 2014 until 16 June 2016 of items starting from a narrow band of locations (the green polygon) near 35°S (upper) and 40°S (lower) on the 7th arc. Trajectories from other bands of starting locations, for various durations, are available in the **[on-line Appendix]**.

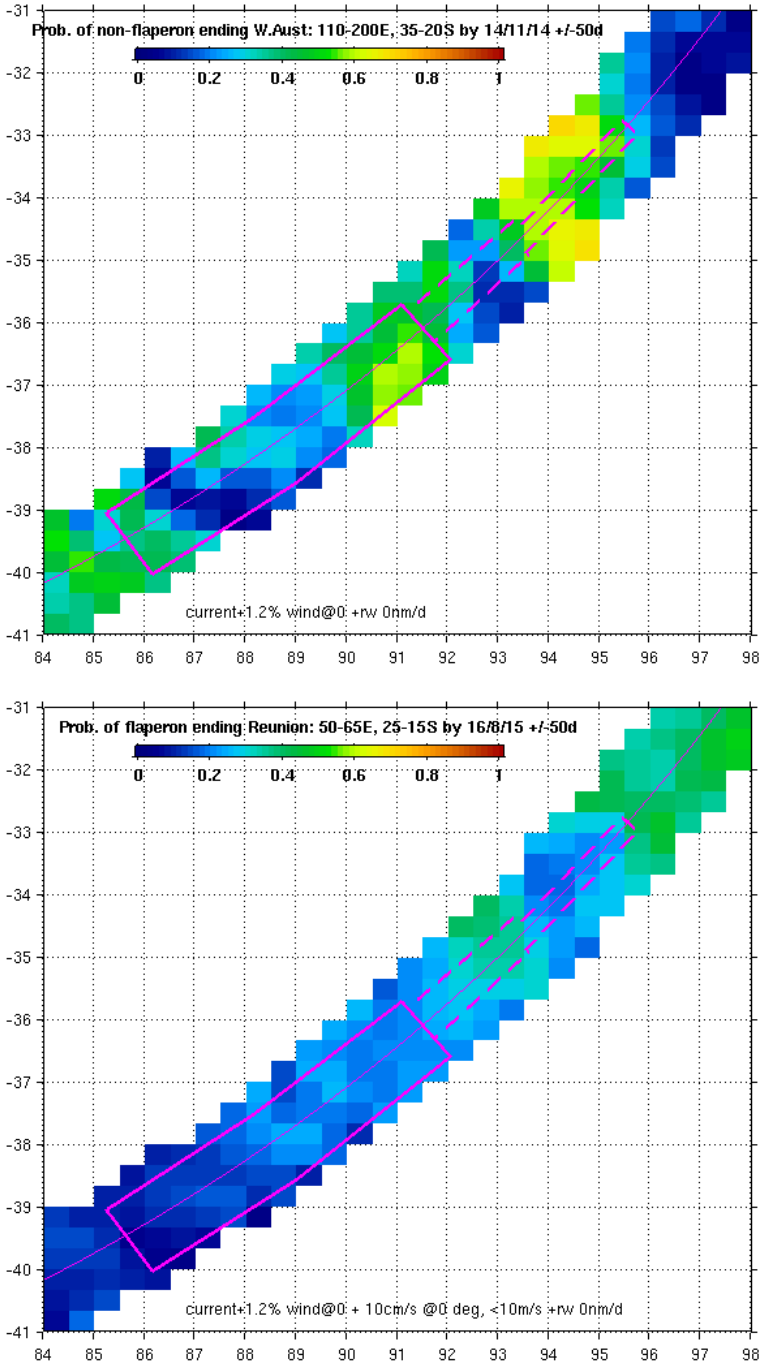


Figure 3.3.3 a) Probability as a function of both latitude and longitude of non-flaperon items being near or on the WA coastline in late 2014, b) probability of flaperon-like items being in the vicinity of Ile de La Reunion around the time that the real flaperon was found.

# 4 The March-April 2014 sea-surface search

The 40-day aerial and vessel-based search of the sea surface for debris from the missing flight was the most extensive aviation accident search ever conducted, yet no wreckage from the aircraft was found. Until parts of the aircraft started being discovered along the coast of Africa, a plausible explanation for the outcome of the surface search was that the aircraft sank in one piece. But we now know, from the large number of small items that have been found, that the aircraft was destroyed on impact. This means we can now use the surface search to indicate where the aircraft was *less* likely to have entered the water, narrowing the range of locations where we need to search the sea floor.

The surface search began on 18 March 2014 with just a few search assets (P3 Orions) being deployed to what is now thought to be the southern limit of the likely area, then finished in what is now thought to be north of the most likely area. Information available at the time never pointed to an intermediate region between these extremes as being a likely location of the aircraft, so one possible interpretation of the outcome of the surface search is that the accident occurred in that intermediate region.

The surface search was guided by estimates of where debris might have been at the time, given an assumed impact location, the elapsed time, and estimates of surface currents, wind and the windage factors of the debris items. We now have better estimates of those latter quantities than were available at the time, so we can evaluate the likelihood of items being found for all possible locations of the aircraft better than we could during the surface search. Daily estimates of the probability of detection (POD) were made by the search coordinators at AMSA based on the weather, number of search assets deployed, the size of the search area and other factors. These estimates of POD assume that there is only a single target being searched, so they are conservative given that there were many items on the sea surface.

Our analysis (Fig. 4.1) shows that the surface search strongly contra-indicates regions north of 32°S as being the location of the accident. It also mildly contra-indicates the region between 34°S and 32°S. The region between 34°S and 38°S emerges as the area where debris from an aircraft impact was highly likely to have escaped detection.

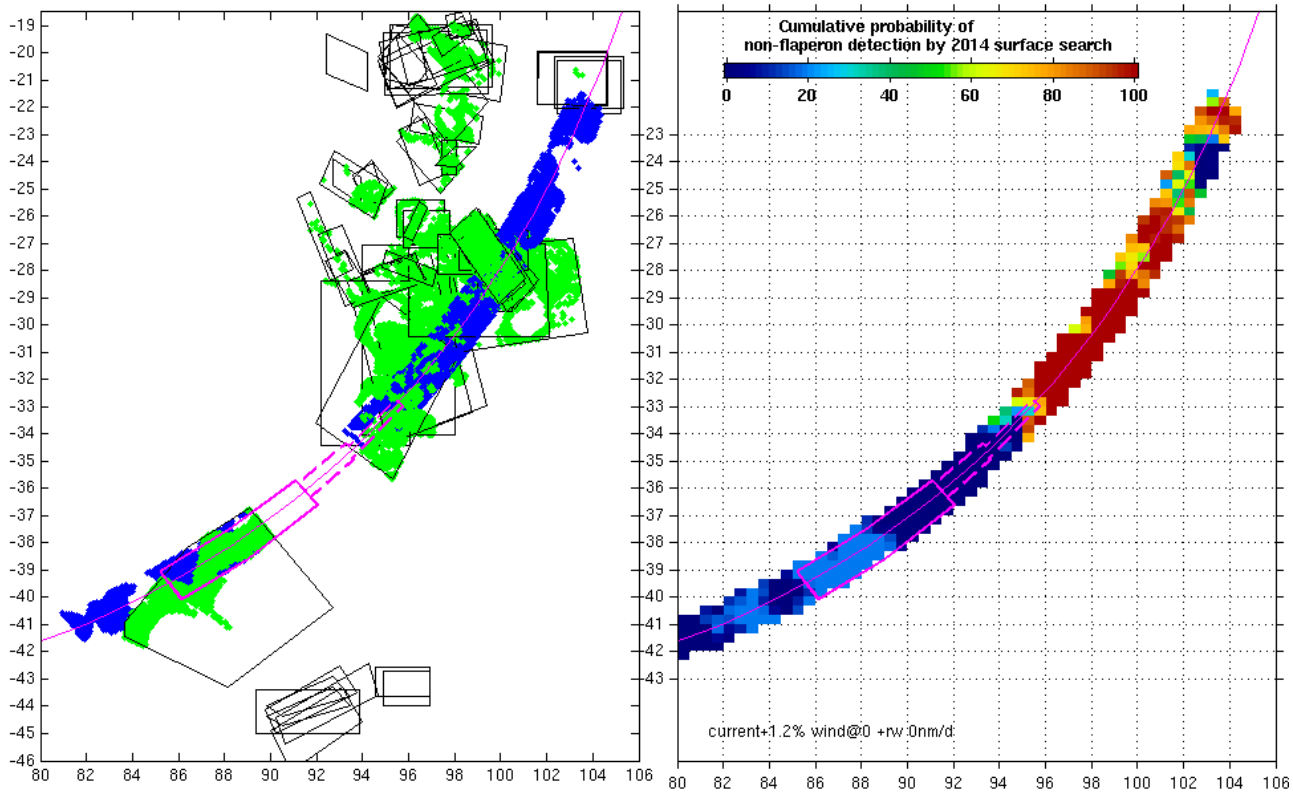


Figure 4.1 Efficacy analysis of the surface search. The left panel shows the daily search areas as black polygons. Locations of potential debris items that were inside a search area on the day it was searched are shown in green, while blue shows where those items were on 8 March 2014. An absence of blue or green near the arc, therefore, indicates areas where trajectories passed through *none* of the surface search boxes. We assume here that potential debris items originated within 45NM of the 7$^{th}$ arc and had an effective windage factor of 1.2%, like the items that eventually washed up in Africa. The right panel shows an estimate of the total efficacy of the search, as a map of the cumulative probability of detection (POD) of potential debris. [online Appendix: results for flaperon-like drift].

# 5 Conclusion

The sea-floor search has all but ruled out the possibility that 9M-MRO lies within ~40NM of the 7th arc between latitudes of 39.3°S to 36°S, or within 10 to 21NM from the arc in segments between 36°S and 32.8°S. Now that we know (from the number and size of items found) that there definitely was a surface debris field, the fact that the sea surface search detected no wreckage argues quite strongly that the site was not between 32°S[2] and 25°S. Those latitudes are also contra-indicated by an absence of aircraft parts being found off Africa earlier than December 2015. Latitudes south of 39°S are quite strongly contra-indicated by the arrival times of the flaperon and other debris reaching Africa, and the fact that those items were many while findings anywhere on the Australian coastline were nil. Latitudes north of 25°S are strongly contra-indicated by the absence of findings on African shores in 2014.

Assuming that the site was within ~25NM of the arc (ATSB 2016), this leaves only points between 36°S and 32°S that are less than ~25NM from the arc but outside the area that was searched in late 2014 and early 2015.

There is a region within the 36-32°S segment of the arc, near 35°S (see Fig. 3.3.3) that is most consistent with all of the following lines of evidence, taken together:

1. absence of detections during the 2014 surface search
2. absence of findings on the WA coastline
3. July 2015 arrival time of the flaperon at La Reunion
4. December 2015 and onwards (only) arrival times of other debris in the western Indian Ocean.

We therefore conclude that while the whole 36°-32°S region (outside the searched area but within the latest estimates of maximum likely off-arc distance) is prospective, the subset region near 35°S appears to be the most likely location of the aircraft.

Can we rule out other locations? Of course not, especially the 33-32°S shoulder region which appears likely from some considerations (lack of WA debris, flaperon finding timing) but less likely from others (African debris timing, surface search). Regions beyond that are much less consistent with available information than the relatively-small remaining prospective region. They are also spread over a very wide region (north, south, east and west) that is far too large to search with present technology.

[2] Latitudes and longitudes specified as integers, or accompanied by the word 'near' in this report have an implied uncertainty of 1/2°

# Appendix A Frequently Asked Questions

**Why don't you do backtracking of the debris?** We have done, but haven't reported it here because it turned out not to be as informative as the forward tracking. The reason is simple: we do not know the exact day when items beached, or even the exact month for some items. To allow for this we had to compute reverse trajectories for many potential arrival dates. The problem is that the 'wrong' ones outnumber the more relevant ones, so the scope for misleading results is great.

**Why are your 'destination' boxes so large?** We can calculate as many model trajectories as we like, but we cannot change the fact that we have a relatively small number of found objects to compare these with. The flaperon that beached on La Reunion, for example, could very well have just missed that island, or it may have missed it by 500 or 1000km due to a chance event that we cannot possibly take account of specifically. So the boxes represent destinations that are equivalent, for the purposes of calculating probabilities.

**Why did you build replica flaperons instead of using a real flaperon?** Flaperons are not easy to obtain, but we are still trying to obtain one. That said, we think the replicas have removed a lot of uncertainty about the drift speed of the real thing.

**Why didn't you do this work earlier?** Many things had to happen before this work could even be started. It was the arrival of many confirmed pieces of wreckage that made oceanographic drift analysis potentially valuable for refining the SatCom estimates. This was significant for two reasons: 1) the arrival times discount northern accident sites, and 2) they confirm the existence of a debris field, which changed the way we interpret the outcome of the surface search, and the absence of Australian findings. Those elements, added to the outcome of the sea-floor search, then directed our focus onto a smaller region, which only then could become further reduced in size by examining the details of the oceanography in March 2014.

**Would the barnacles have slowed things down?** Relative to the water, yes. But this is a very small speed anyway. Most of the downwind drift is due to Stokes Drift, which carries a submerged clump of barnacles or seaweed at the same speed as a clean piece of aircraft fuselage.

**What if you used a different ocean model?** We have also used a version of our model that only became available at the very end of the project. Details of results are different (because the eddies in the model are chaotic, just like in the real ocean) but all the conclusions remained the same. Both models are informed by the same satellite data so they do not differ significantly.

# Glossary

**7th arc**. The curved line defined by a set of points that are all a certain distance from the Inmarsat satellite via which 9M-MRO was in communication with a satellite ground station. This distance is inferred from the Burst Timing Offset associated with the 7th communication since losing contact with traffic controllers. For more detail, see ATSB 2015.

**9M-MRO**. The designation of the particular Boeing 777 aircraft flying as Malaysian Airlines Flight MH-370.

**Altimeter**. An instrument carried by an earth-observation satellite that measures two quantities extremely accurately – 1) its position in space and 2) the distance to the surface of the ocean directly below – in order to estimate the departure of the sea surface from a reference surface. This project used data from the following missions operated by the respective space agencies: Jason-2 (NASA and CNES), CryoSat2 (ESA), AltiKa (CNES and ISRO). FFI see http://oceancurrent.imos.org.au/glossary.php

**BFO**. Burst Frequency Offset, a measure of the Doppler shift due to the satellite-aircraft velocity difference resolved along the line joining the two.

**Extrados**. The upper surface of a wing (the **Intrados** is the lower surface).

**Draft**. The distance below the waterline of the lowest point of a floating object.

**Freeboard**. The distance above the waterline of a floating object.

**Flaperon**. A flight control surface on the trailing edge of an aircraft wing that combines the functions of both flaps and ailerons. The flaperons are primarily used to improve stability during low-speed take-off and landing flight phases. The Boeing 777-200 flaperon is constructed from a lightweight composite structure that floats in water.

**GDP.** Global Drifter Program, housed at the US National Oceanic and Atmospheric Administration Atlantic Oceanographic and Meteorological Laboratory (NOAA AOML). FFI see http://www.aoml.noaa.gov/phod/dac/gdp_information.php

**NM**. Nautical mile. Equivalent to one minute of latitude, or 1.85km.

**SatCom**. Satellite communication between the aircraft and ground stations via an Inmarsat satellite. In the present case, this refers to system-initiated handshake signals, but no transmission of any user or engineering data.

**SLDMB**. Self-Locating Datum Marker Buoy. A type of surface drifter used by operational agencies. It drifts at the velocity of the upper 70cm of the ocean with essentially zero windage, so it is different to GLD drifters in both their drogued and undrogued states.

**SVP drifter**. Surface Velocity Program drifter. These are used by the GDP. In this document we call these 'GDP drifters'.

**Stokes Drift**. Movement in the direction of waves due to the fact that the orbital velocity of a parcel of water, due to the passage of a wave, is not a closed ellipse.

**Windage**. Strictly speaking, this is defined as the wind-driven motion with respect to the water of a floating object, due to the force of the wind on the object. More commonly, it is taken to be the wind-driven motion with respect to specific measure of the surface velocity. If that measure does not include the Stokes Drift or other wind-related quantities, then the windage factor (ratio of windage to wind speed) will be a measure of them too.

# References


Ardhuin FL, Marié N, Rascle N, Forget P, Roland A (2009) Observation and estimation of Lagrangian, Stokes and Eulerian currents induced by wind and waves at the sea surface. *Journal of Physical Oceanography* **39(11)**, 2820-2838.

ATSB (2015) MH370 – Definition of underwater search areas. ATSB, 3, 10 December 2015.

ATSB (2016) MH370 – Search and debris examination update. ATSB, 2 November 2016.

Dee DP, Uppala S (2009) Variational bias correction of satellite radiance data in the ERA-interim reanalysis. *Quarterly Journal of the Royal Meteorological Society* **135 (644)**, 1830-184.

Durgadoo JV, Biastoch A (2015) Where Is MH370? GEOMAR Helmholtz Centre for Oceanic Research Kiel, Press Release 44, 2015. http://www.geomar.de/en/service/kommunikation/singlepm/article/wo-ist-mh370

Durgadoo JV, Rühs S, Biastoch A, Nurser AJG, New AL, Drillet JHY, Durand E, Rodwell MJ, Bidlot JR, Janssen PAEM (2016) Backtracking of the MH370 flaperon from La Réunion, GEOMAR, May 2016

Jansen E, Coppini G, Pinardi N (2016) Drift simulation of MH370 debris using superensemble techniques. *Natural Hazards and Earth Systems Sciences* **16**, 1623-1628. doi: 10.5194/nhess-16-1623-2016

Pattiaratchi C, Wijeratne S (2016) Ocean currents suggest where we should be looking for missing flight MH370. *The Conversation*, 28 July 2016.

Lumpkin R, Grodsky SA, Centurioni L, Rio MH, Carton JA, Lee D (2013). Removing spurious low-frequency variability in drifter velocities, *Journal of Atmospheric and Oceanic Technology* **30**, 353-360. doi: JTECH-D-12-00139

Oke PR, Sakov P, Cahill ML, Dunn JR, Fiedler R, Griffin DA, Mansbridge JV, Ridgway KR, Schiller A (2013a) Towards a dynamically balanced eddy-resolving ocean reanalysis: BRAN3. *Ocean Modelling* **67**, 52-70, doi: dx.doi.org/10.1016/j.ocemod.2013.03.008

Oke PR, Griffin DA, Schiller A, Matear RJ, Fiedler R, Mansbridge JV, Lenton A, Cahill M, Chamberlain MA, Ridgway K (2013b) Evaluation of a near-global eddy-resolving ocean model. *Geoscientific Model Development* **6**, 591-615, doi:10.5194/gmd-6-591-2013.

Pengam (2016) Simulations de polaires aerodynamiques et hydrodynamics (Lot 2) *in* Essai de flottabilite pour DGA TA. Direction Generale de l'Armement. DGA Techniques hydrodynamics. No 16-500-560 DT/DGA TH/SDT/UP_PERF du 1/4/2016.

Polton JA, Lewis DM, Belcher SE (2005) The role of wave-induced Coriolis-Stokes forcing on the wind-driven mixed layer. *Journal of Physical Oceanography* **35**, 444-457.

Rascle N, Ardhuin F (2013) A global wave parameter database for geophysical applications. Part 2: Model validation with improved source term parameterization. *Ocean Modell* **70**, 174-188 http://dx.doi.org/10.1016/j.ocemod.2012.12.001

Röhrs J, Christensen KH, Hole LR, Broström G, Drivdal M, Sundby S (2012). Observation-based evaluation of surface wave effects on currents and trajectory forecasts. *Ocean Dynamics* **62**, 1519-1533, doi:10.1007/s10236-012-0576-y

Trinanes JA, Olascoaga MJ, Goni GJ, Maximenko NA, Griffin DA, Hafner J (2016) Analysis of flight MH370 potential debris trajectories using ocean observations and numerical model results, *Journal of Operational Oceanography*, doi: 10.1080/1755876X.2016.1248149

Vozchikov L, Selena L (2016) Experimental drift mapping of Indian Ocean gyre aircraft debris. *Open Journal of Applied Sciences*, **6**, 95-99. doi: 10.4236/ojapps.2016.62010

CONTACT US

**t** 1300 363 400
+61 3 9545 2176
**e** csiroenquiries@csiro.au
**w** www.csiro.au

AT CSIRO, WE DO THE EXTRAORDINARY EVERY DAY

We innovate for tomorrow and help improve today – for our customers, all Australians and the world.

Our innovations contribute billions of dollars to the Australian economy every year. As the largest patent holder in the nation, our vast wealth of intellectual property has led to more than 150 spin-off companies.

With more than 5,000 experts and a burning desire to get things done, we are Australia's catalyst for innovation.

CSIRO. WE IMAGINE. WE COLLABORATE. WE INNOVATE.

FOR FURTHER INFORMATION

**CSIRO Oceans and Atmosphere**
David Griffin
**t** +61 3 6232 5244
**e** David.Griffin@csiro.au
**w** www.csiro.au